



HAL
open science

Quantum Rényi entropy by optimal thermodynamic integration paths

Miha Srđinšek, Michele Casula, Rodolphe Vuilleumier

► **To cite this version:**

Miha Srđinšek, Michele Casula, Rodolphe Vuilleumier. Quantum Rényi entropy by optimal thermodynamic integration paths. *Physical Review Research*, 2022, 4 (3), pp.L032002. 10.1103/PhysRevResearch.4.L032002 . hal-03779480

HAL Id: hal-03779480




<https://hal.science/hal-03779480>

Submitted on 16 Sep 2022

HAL is a multi-disciplinary open access archive for the deposit and dissemination of scientific research documents, whether they are published or not. The documents may come from teaching and research institutions in France or abroad, or from public or private research centers.

L'archive ouverte pluridisciplinaire **HAL**, est destinée au dépôt et à la diffusion de documents scientifiques de niveau recherche, publiés ou non, émanant des établissements d'enseignement et de recherche français ou étrangers, des laboratoires publics ou privés.

Quantum Rényi entropy by optimal thermodynamic integration paths

Miha Srdinšek ^{1,2,3,*}, Michele Casula ², and Rodolphe Vuilleumier ³

¹*Institut des sciences du calcul et des données (ISCD), Sorbonne Université, 4 Place Jussieu, 75005 Paris, France*

²*Institut de minéralogie, de physique des matériaux et de cosmochimie (IMPMC), Sorbonne Université, CNRS UMR 7590, MNHM, 4 Place Jussieu, 75005 Paris, France*

³*Processus d'Activation Sélectif par Transfert d'Énergie Uni-électronique ou Radiative (PASTEUR), CNRS UMR 8640, Département de Chimie, École Normale Supérieure, 24 rue Lhomond, 75005 Paris, France*



(Received 29 December 2021; accepted 9 June 2022; published 5 July 2022)

Despite being a well-established operational approach to quantify entanglement, Rényi entropy calculations have been plagued by their computational complexity. We introduce here a theoretical framework based on an optimal thermodynamic integration scheme, where the Rényi entropy can be efficiently evaluated using regularizing paths. This approach avoids slowly convergent fluctuating contributions and leads to low-variance estimates. In this way, large system sizes and high levels of entanglement in model or first-principles Hamiltonians are within our reach. We demonstrate this approach in the one-dimensional quantum Ising model and perform an evaluation of entanglement entropy in the formic acid dimer, by discovering that its two shared protons are entangled even above room temperature.

DOI: [10.1103/PhysRevResearch.4.L032002](https://doi.org/10.1103/PhysRevResearch.4.L032002)

Introduction. Measuring the entanglement of a quantum state or the entropy of a quantum system at thermal equilibrium has always been a challenge. With the aim of achieving this goal, several methods have been proposed so far [1–9]. One of the most promising approaches is based on the evaluation of the quantum Rényi entropy. For subsystem A of a quantum system, it is defined as [1,10–12]

$$S_A^\alpha = \frac{1}{1-\alpha} \ln \frac{\text{Tr} \rho_A^\alpha}{[\text{Tr} \rho]^\alpha}, \quad (1)$$

where ρ and ρ_A are density matrices of the full system and of its subsystem A , respectively, with $\alpha \in \mathbb{R}_{>0} \setminus \{1\}$. When ρ_A equals the full density matrix ρ , S_A^α serves as a very general signature of thermodynamic phase transitions. Moreover, when a smaller subsystem is considered, it can detect quantum phase transitions [2,3,13–20] occurring at zero temperature and quantifies the entanglement of the ground state. Together with its derivatives, such as mutual information [15], topological entropy [21], or simply entropic inequalities [1,12,22], it can be used to classify different ground states and topological phases, extract critical exponents, and study thermalization under unitary time evolution [23–25].

Despite being a fundamental proxy to understand the thermodynamics of quantum systems, the Rényi entropy is not measurable in experimental setups, apart from rare successes [22,26]. The same holds for the Rényi entropy

evaluation via analytical treatments or numerical methods, such as the density matrix renormalization group (DMRG) and stochastic sampling frameworks [2–5,9,18,27,28]. In the former case, Rényi entropy evaluation is limited mostly to integrable models [14,29–32], while in the latter, it is limited to low-dimensional systems with sufficiently low entanglement [33–35]. Quantifying the Rényi entropy in more general complex systems has remained so far an unattainable task, hampered by the exponentially high energy barriers in stochastic sampling frameworks.

Of particular interest are hydrogen-rich materials, such as liquid water [36], where quantum effects arise due to the light mass of hydrogen. It has been shown that nuclear quantum effects pilot phase transitions in these systems, leading, for instance, to phase VIII of water ice and to the superconducting phases of hydrides, such as LaH_{10} [37], YH_n [38], and H_3S [39]. For the same reasons, entanglement is supposed to play a role also in biochemical systems, such as the formic acid dimer [40–43] and base pairs in DNA [44–46].

In this Research Letter, we present an alternative approach that overcomes previous limitations and allows one to compute the Rényi entropy S_A^α for complex quantum systems, described by either model or *ab initio* Hamiltonians. The latter is demonstrated by producing evidence of entanglement in the formic acid dimer. Our approach is based on the combination of the path integral (PI) formalism and thermodynamic integration along appropriately defined paths.

Rényi entropy with path integrals. In the PI formulations of statistical mechanics, the quantum density matrix ρ at time t is mapped to a classical counterpart by Wick-rotating ($t \rightarrow -i\beta$) the quantum action and discretizing it into a classical Hamiltonian H [47,48]. In practical implementations, the imaginary time interval $[0, \beta = 1/(k_B T)]$, T being the temperature, is divided into a finite number of time steps,

*miha.srdinsek@upmc.fr

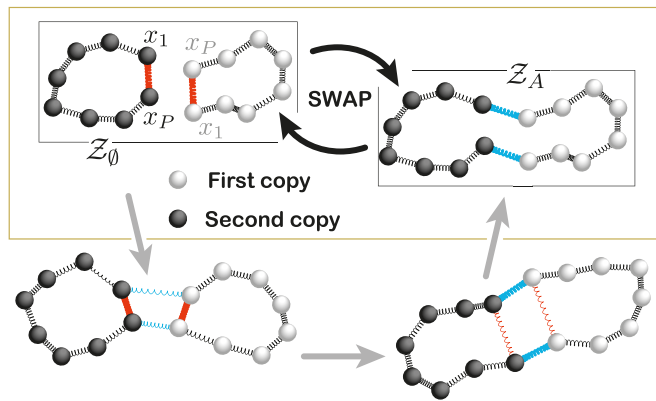


FIG. 1. \mathcal{Z}_\emptyset and \mathcal{Z}_A for a quantum particle with $\alpha = 2$ are shown in the upper boxes. S^2 can then be computed by averaging the “SWAP” operator or by introducing intermediate steps (gray arrows) and averaging the spring interactions highlighted in colors (red, blue) over an appropriately defined path. The springs’ strength is proportional to color intensity.

which are individual snapshots (or beads) that interact in a particlewise manner in the imaginary time direction. One can then use importance sampling algorithms to evaluate the Rényi entropy of $\alpha \in \mathbb{N} \setminus \{1\}$ by calculating the free-energy difference between two statistical ensembles, namely, $S_A^\alpha = \ln(\mathcal{Z}_A/\mathcal{Z}_\emptyset)/(1 - \alpha)$ [14]. $\mathcal{Z}_\emptyset = [\text{Tr}\rho]^\alpha$ is the partition function of the \emptyset ensemble, consisting of α independent copies of the system, and $\mathcal{Z}_A = \text{Tr}\rho_A^\alpha$ is the one for the joint ensemble, where each particle belonging to subsystem A is replaced by one particle living in all the α copies. Thus Rényi entropy depends only on the free-energy cost of changing the boundary conditions through the “SWAP” operator (see Fig. 1) in the imaginary time direction.

This free-energy cost can be estimated by running a PI Monte Carlo simulation in one ensemble, say, \mathcal{Z}_\emptyset , and averaging the exponent of the energy difference between the two boundary conditions at given β [2,8,49], in order to evaluate

$$\ln\left(\frac{\mathcal{Z}_A}{\mathcal{Z}_\emptyset}\right) = \ln\langle \exp[-\beta(H_A - H_\emptyset)] \rangle_{\mathcal{Z}_\emptyset}. \quad (2)$$

$H_{A,\emptyset}$ are classical Hamiltonians arising from the discretization of their corresponding quantum actions $\mathcal{Z}_{A,\emptyset}$. Though Eq. (2) is in principle exact, it implies that for increasing energy differences one has to wait exponentially longer times to sample high-energy configurations. A possible remedy for this slowing down is to split the calculation into shorter increments of smaller free-energy differences [2] and to sample the ratio of the Metropolis-Hastings transition probabilities $\langle \min(1, \exp(-\beta\Delta H)) \rangle_{\mathcal{Z}_\emptyset} / \langle \min(1, \exp(\beta\Delta H)) \rangle_{\mathcal{Z}_A}$ [50,51], rather than Eq. (2). Following these procedures, reliable and groundbreaking entanglement entropy estimations were obtained in one-dimensional (1D) and two-dimensional (2D) spin chains [3,9], and cold atoms [27]. Nevertheless, in larger or more strongly entangled systems, the consequently higher energy barriers can cause the aforementioned approach to fail.

Thermodynamic integration. An alternative scheme is the thermodynamic integration based on a new partition function

$\mathcal{Z}[\lambda]$, a differentiable function of the parameter $\lambda \in [0, 1]$, that connects the two ensembles [5,8]. Then, by using the relation

$$\ln\left(\frac{\mathcal{Z}_A}{\mathcal{Z}_\emptyset}\right) = -\beta \int_0^1 \langle \partial_\lambda H(\lambda) \rangle_{\mathcal{Z}[\lambda]} d\lambda \quad (3)$$

and setting $\mathcal{Z}[0] = \mathcal{Z}_\emptyset$ and $\mathcal{Z}[1] = \mathcal{Z}_A$, one evaluates the entropy by sampling the derivative of the $H(\lambda)$ Hamiltonian appearing in $\mathcal{Z}[\lambda]$ and avoiding the exponential function present in Eq. (2). Usually, the line integral in Eq. (3) is performed numerically on a finite mesh. A common choice, previously used in the literature [52], is taking an integration path that leads to $H(\lambda) = H_\emptyset + \lambda(H_A - H_\emptyset)$. According to Eq. (3), then one has to average the energy difference $H_A - H_\emptyset$ over the $\mathcal{Z}[\lambda]$ ensemble. A representation of the λ -dependent part of $H(\lambda)$ is highlighted in color in Fig. 1. However, it was observed [52] that the final value for the entropy is the result of an almost perfect cancellation between two possibly large contributions of opposite sign coming from $\lambda < 1/2$ and $\lambda > 1/2$, respectively. Moreover, at high temperature the integrand $\langle H_A - H_\emptyset \rangle_{\mathcal{Z}[\lambda]}$ diverges at the edges of the integration path [see Fig. 2(c)]. Thus, to get reliable results, high precision and a large number of integration steps are needed. The thermodynamic integration based on the simplest integration path is therefore also doomed to failure when faced with large systems [3].

In order to understand the origin of these drawbacks, we focus on the harmonic oscillator and its Rényi entropy of second order (i.e., with $\alpha = 2$), the exactly solvable minimal model, where the behavior is reproduced. In the PI formulation of \mathcal{Z}_\emptyset , each copy of the quantum harmonic oscillator of mass m and frequency ω is described by a ring polymer with beads $\{x_k\}_{k=1,\dots,P}$ connected by harmonic springs [48], such that

$$H = \frac{m}{2} \sum_{k=1}^P \left[\frac{1}{\zeta^2 \hbar^2 P} (x_{k+1} - x_k)^2 + \frac{\omega^2}{P} x_k^2 \right] \Bigg|_{x_{P+1}=x_1}. \quad (4)$$

In the following, we will solve this model for $m = 1$ and $\omega = 1$. In Eq. (4), $\zeta = \beta/P$ is the imaginary time step which controls the discretization error and represents the inverse temperature of the classical analog. Switching from the split ensemble to the joint one amounts to neglecting the harmonic interaction in H_\emptyset between the beads x_P and x_1 in both copies, and adding the interaction between x_P of the first copy and x_1 of the second one, and its crossed term, in H_A (see Fig. 1). The average energy of the joint interaction computed over \mathcal{Z}_\emptyset is greater than the split one, because copies do not interact with each other in \mathcal{Z}_\emptyset and thus they can be at relatively large distances. This contribution grows with the square of the interbead distance and with the phase-space size. Moreover, as the temperature increases, the interaction energy grows as $1/\beta$ and the de Broglie wavelength shrinks. Copies collapse to almost pointlike particles, and this further contributes to the diverging cost of joining them. This shows up in the large value of the integrand at $\lambda = 0$ in the simplest integration scheme. Similarly, the variance of this contribution is large, since \mathcal{Z}_\emptyset minimizes the action without $H_A - H_\emptyset$. An analogous contribution but of opposite sign appears at $\lambda = 1$, further increasing the overall uncertainty of the integral. Nevertheless, we found that if a more general path is considered,

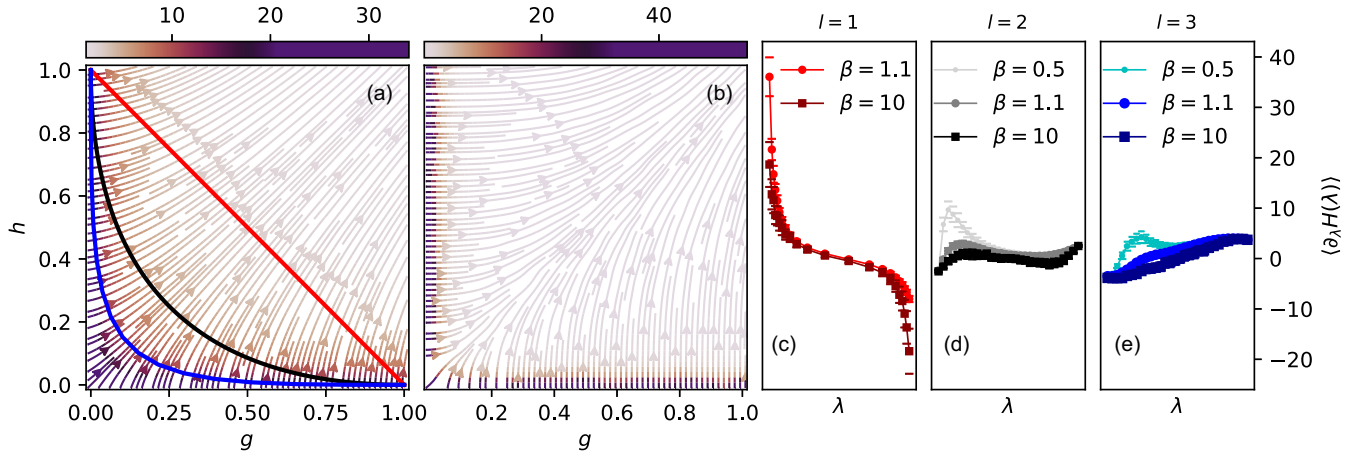


FIG. 2. (a) Stream plot of the gradient field ($\langle K_\theta \rangle_{Z[\lambda]}$, $\langle K_A \rangle_{Z[\lambda]}$) for the single-particle 1D harmonic oscillator at $\beta = 10$ as a function of (g, h) . Colors indicate the magnitude of the gradient, according to the palette above the frame. (b) Stream plot of the variance field ($\text{var}[K_\theta]$, $\text{var}[K_A]$). The black (blue) line in (a) represents the path in Eq. (7) with $l = 2$ ($l = 3$). The red line in (a) is the linear path ($l = 1$). Changing the path from linear to black or to blue regularizes the integrand by cutting off its spikes at the edges, shown at different temperatures for $l = 1, 2, 3$ in (c), (d), and (e), respectively.

the pathological behavior of the integrand at the edges and its large variance can be avoided altogether.

Path regularization. In search of enhanced paths, we focus on the 2D parameter space (g, h) of Hamiltonians $H(g, h) = H_\theta + (g - 1)K_\theta + hK_A$. The $K_{\theta,A}$ operators correspond to the interactions that enforce the boundary conditions: K_θ (K_A) drives the intracopy (intercopy) closure of the particle rings. These terms are depicted in red (blue) in Fig. 1. Different paths connecting $(1,0)$ ($H = H_\theta$) to $(0,1)$ ($H = H_A$) can be compared by inspecting the gradient field of the energy $\mathbf{K} \equiv (\partial H/\partial g, \partial H/\partial h) = (\langle K_\theta \rangle_{Z[\lambda]}, \langle K_A \rangle_{Z[\lambda]})$, and the corresponding variance field $\text{var}[\mathbf{K}] \equiv (\text{var}[K_\theta], \text{var}[K_A])$ in the (g, h) plane, shown in Figs. 2(a) and 2(b), respectively. At each (g, h) point, the direction of the field indicates the path $\mathbf{p} \equiv (g(\lambda), h(\lambda))$ that would yield the largest possible increment or the largest possible uncertainty to the line integral in Eq. (3), with magnitude represented by the color of the stream plot. For the 1D harmonic oscillator [Fig. 2(c)], we can clearly see that the path connecting linearly the two endpoints, i.e., the one that has commonly been employed so far, produces two spikes in $\langle \partial_\lambda H(\lambda) \rangle_{Z[\lambda]}$ at $(1,0)$ and $(0,1)$, exactly where the scalar product of the path direction ($\mathbf{p}' \equiv \partial_\lambda \mathbf{p}$) with the gradient field is the largest. This is understood once the integral in Eq. (3) is recast in $-\beta \int_0^1 \mathbf{p}' \cdot \mathbf{K} d\lambda$. The origin of spikes can be traced down to the K_A growth along $(g, 0)$ and K_θ growth along $(0, h)$, as the temperature increases. These drawbacks are present in any system where intrabead interaction is large. In order to remove the spikes, one should therefore avoid moving towards directions where previously nonexistent interactions are switched on in $H(g, h)$.

This analysis suggests that the optimal integration path is the one which minimizes

$$F_{\text{Abs}}[\mathbf{p}] = \frac{1}{\int |\mathbf{p}'| d\lambda} \int_0^1 |\mathbf{p}' \cdot \mathbf{K}| d\lambda \quad (5)$$

over the entire path. Another criterion can be derived by minimizing the full variance [53], which implies the line min-

imization of

$$F_{\text{Variance}}[\mathbf{p}] = \int_0^1 ((\partial_\lambda g)^2, (\partial_\lambda h)^2) \cdot \text{var}[\mathbf{K}] d\lambda. \quad (6)$$

Either choice makes the integrand flat as a function of λ . This scheme acts therefore as a *path regularization*. Not only are the spikes at the endpoints cut off, but also the line integral can be computed on a much coarser grid, speeding up the calculation and reducing both deterministic and stochastic errors.

It is clear that the full path optimization would not be affordable in the most general case. However, the simple 1D quantum oscillator, where the path search can be carried out systematically, provides a shape that is transferable to complex quantum many-body systems. \mathbf{p} can then be parametrized as a differentiable curve:

$$(g(\lambda), h(\lambda)) = ((1 - \lambda)^l, \lambda^l) \quad \text{with } \lambda \in [0, 1]. \quad (7)$$

If rescaled by the proton mass, the reported behavior of the 1D harmonic oscillator spans a physically relevant range of parameters with temperatures going from 4.3 K ($\beta = 40$) to 344 K ($\beta = 0.5$) and with a vibrational frequency of 5122 cm^{-1} . In this realistic regime, it turns out that $l = 2$ optimizes the path based on $|\mathbf{p}' \cdot \mathbf{K}|$ [Fig. 3(a)], while $l = 3$ is the optimal power law based on $\text{var}[\mathbf{K}]$ [Fig. 3(b)]. Nevertheless, the latter is the best choice in *ab initio* systems over a large range of temperatures [53]. Indeed, these systems have an intrabead interaction similar to that of the harmonic oscillator studied above, provided by the quantum kinetic term of the *ab initio* action.

1D Ising model in a transverse magnetic field. The harmonic oscillator is, however, a too simple model to possess any entanglement. In a system with a larger number of interacting particles, the coefficients (g, h) change the boundary condition of the full subsystem. To explicitly check the generality of the *path regularization* approach, we now study the 1D Ising model in a transverse magnetic field with periodic

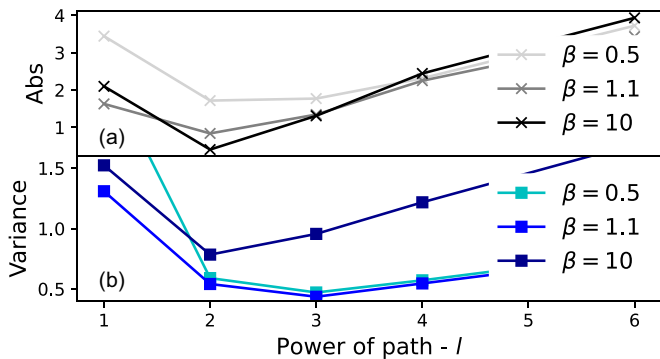


FIG. 3. Cost functionals [53] estimating the (a) excess area under the integrand [F_{Abs} from Eq. (5)] and (b) variance of the integral [F_{Variance} from Eq. (6)] for different regularizing paths defined by the parameter l . Three values of the temperature are shown.

boundary conditions. Its Hamiltonian reads

$$H = \sum_i \sigma_i^z \sigma_{i+1}^z + r \sigma_i^x, \quad (8)$$

where $\sigma_i^{x,z}$ are Pauli matrices acting on the i th site and r is the strength of the magnetic field in the x direction. Due to its integrability (it can be analytically solved using Jordan-Wigner transformation [54]), it represents an ideal benchmark for our path regularization in an extended system. It undergoes a quantum phase transition at $r = 1$.

Within the PI framework, Eq. (8) is mapped into the 2D classical anisotropic Ising model [53]. The interaction in the imaginary time direction of the classical counterpart diverges as $r \rightarrow 0$, causing effects analogous to the temperature increase in the harmonic oscillator. At small r , the path in Eq. (7) successfully kills large fluctuations appearing at the endpoints if $l = 3$ is used. In this case, there is still room for improving the thermodynamic integration path. Indeed, in this model system, the magnitude of the endpoints still grows with the interaction strength. This can be cured by rescaling the λ parameter [53], which provides an additional freedom to optimize the path. Rescaling λ leaves the shape of the path unchanged, but it varies the “speed” (i.e., the integration points’ density) along the thermodynamic trajectory. To compare our method with sampling algorithms based on the SWAP operator [Eq. (2)], such as the one in Ref. [3], we computed the Rényi entropy of second order S_{full}^2 with the whole system as a subsystem. This quantity is the hardest to evaluate. The full entropies obtained with the SWAP scheme and the *path regularization* both agree well with analytical results over a wide range of magnetic field strengths (Fig. 4). S_{full}^2 nicely captures the quantum phase transition at $r = 1$, by showing a clear peak. In order to estimate the maximum system size that the *path regularization* procedure can afford, we pushed the entropy calculation to very long spin chains, where the thermodynamic limit is reached. In the limit of large L , the full entropy scales as L . From the inset of Fig. 4, it can be seen that this limit is reached at relatively small system sizes. It is also seen that our procedure outperforms the SWAP-based one, since the former can still be applied to systems larger than 600 sites where S_{full}^2 exceeds the value of 50, while the latter is broken already before 400 sites [3]. Indeed, one of the strengths of the path regularization method is that the number

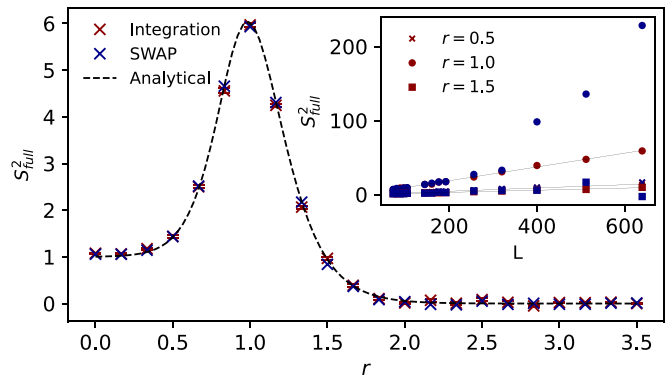


FIG. 4. Ising model. r dependence of the full Rényi entropy of second order [$S_{\text{full}}^2/\ln(2)$] computed with thermodynamic integration via path regularization (red crosses) and transition probability sampling based on the SWAP operator (blue crosses) compared with analytical results (dashed black line) for $L = 64$ and $\beta = 3$. Inset: Comparison of the system-size scaling for the two methods at different r .

of integration steps remains constant with the subsystem size. By increasing the level of entanglement, the time cost grows linearly, while in methods based on Eq. (2), it grows exponentially.

A realistic system: The formic acid dimer. By means of the *path regularization* scheme, the calculation of the Rényi entropy for realistic systems becomes feasible. As an illustrative example, we take here the formic acid dimer, a minimal model of biochemical physics. This is a system of two molecules that form a dimer via a double hydrogen bond [Fig. 5(c)]. Due to the 180° rotation symmetry around the axis connecting the carbon atoms, the potential energy surface (PES) has two minima, which correspond to the two hydrogen configurations shown in Fig. 5. They are separated by a barrier that grows with the interdimer distance d between the oxygen atoms ($d = 2.7 \text{ \AA}$ in equilibrium [41,55]), which determines also the hydrogen bond stretch. During the double proton transfer the two molecules get closer, as close as $d = 2.4 \text{ \AA}$, and the barrier dwindles. Due to the light hydrogen mass, at intermediate distances the quantum effect become prominent [40–43], and the barrier is low enough that the two configurations are expected to be entangled, leading to a concerted motion of the protons.

In our simulations, we restricted the protons to move along the hydrogen bond, and we evaluated the PES as a function of d by means of the coupled-cluster method with single, double, and perturbative triple excitations [CCSD(T)] [53]. At each distance, we ran a PI Monte Carlo simulation of the two protons in a projected PES with our thermodynamic integration scheme [61]. As the potential is simple enough, the outcome of these simulations can be compared against results obtained with the exact diagonalization in a discretized space. This comparison further assesses the robustness of the *path regularization* in Eq. (7), with the optimal power of $l = 3$ for *ab initio* systems. Since the Rényi entropy of the two-proton subspace (“full” entropy) is nonzero at distances where the system is in a mixed state, we can extract a lower bound for quantum correlations [56] by computing the difference between the full entropy and the Rényi entropy of the single-

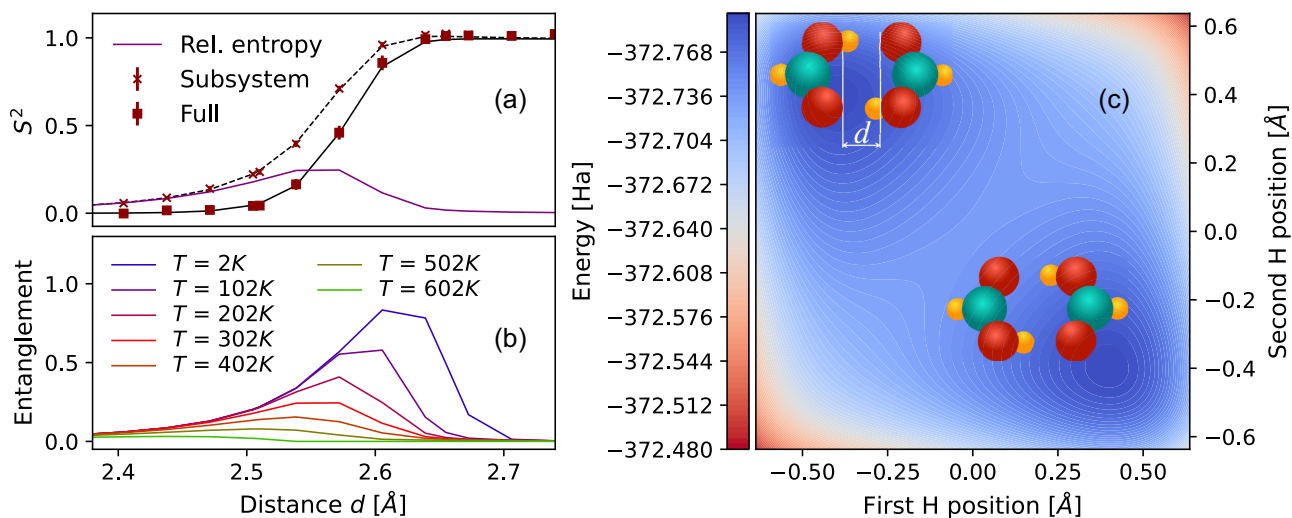


FIG. 5. (a) Full (black solid line) entropy and the entropy of a single-proton subspace [$S_A^2/\ln(2)$] (black dashed line) as a function of the distance d between the formic acid molecules at 300 K. The difference between the two (“relative entropy”)—the lower bound of entanglement—is also shown (purple solid line). (b) Temperature dependence of the relative entropy. (c) 2D PES spanned by the position of the hydrogen atoms along the hydrogen bonds at $d = 2.87$ Å. Rel., relative.

proton subspace (entanglement entropy if in a pure state). The results show that the entanglement is present along the full range of distances, explored during the double proton transfer ($d = 2.4$ – 2.7 Å [41]). However, the temperature plays a major role. At room temperature the entanglement is considerably lower compared with the one at 100 K. Remarkably, it persists up to temperatures as large as 500 K for some intermolecular distance. We note that at high temperatures the thermal motion of the full molecular complex must be taken into account. Nevertheless, the effect is so strong that the entanglement should still be relevant well above room temperature even in this case.

Conclusions. In this Research Letter, we introduced a path regularization scheme that allows an efficient and stable calculation of the quantum Rényi entropy via a thermodynamic integration performed within the path integral framework. The proposed regularization defines an optimal thermodynamic path that smoothly changes the imaginary time boundary conditions of the quantum partition function, by avoiding slowly convergent contributions and by yielding a low-variance estimate of the Rényi entropy. The method has been shown to

be efficient in the 1D Ising model with a transverse magnetic field, where we reached very large subsystem sizes. It also allowed us to perform an *ab initio* evaluation of the Rényi entropy for the concerted hydrogen motion in the formic acid dimer. The path regularization makes the evaluation of the Rényi entropy feasible for model and real systems, comprising large sizes and/or complex interactions, for which the Rényi entropy analysis was previously inaccessible.

The code used in this Research Letter may be accessed [61].

Acknowledgments. We are thankful for the support of the HPCaVe computational platform of Sorbonne University, where the main calculations were performed. We are grateful for the environment provided by ISCD and its MAESTRO junior team. This work was partially supported by the European Centre of Excellence in Exascale Computing TREX-Targeting Real Chemical Accuracy at the Exascale, funded by the European Union’s Horizon 2020 Research and Innovation program under Grant Agreement No. 952165.

- [1] R. Horodecki, P. Horodecki, M. Horodecki, and K. Horodecki, Quantum entanglement, *Rev. Mod. Phys.* **81**, 865 (2009).
- [2] M. B. Hastings, I. González, A. B. Kallin, and R. G. Melko, Measuring Renyi Entanglement Entropy in Quantum Monte Carlo Simulations, *Phys. Rev. Lett.* **104**, 157201 (2010).
- [3] S. Humeniuk and T. Roscilde, Quantum Monte Carlo calculation of entanglement Rényi entropies for generic quantum systems, *Phys. Rev. B* **86**, 235116 (2012).
- [4] V. Alba, Out-of-equilibrium protocol for Renyi entropies via the Jarzynski equality, *Phys. Rev. E* **95**, 062132 (2017).
- [5] J. D’Emidio, Entanglement Entropy from Nonequilibrium Work, *Phys. Rev. Lett.* **124**, 110602 (2020).
- [6] R. P. White and H. Meirovitch, A simulation method for calculating the absolute entropy and free energy of fluids: Application to liquid argon and water, *Proc. Natl. Acad. Sci. USA* **101**, 9235 (2004).
- [7] H. Do and R. J. Wheatley, Density of states partitioning method for calculating the free energy of solids, *J. Chem. Theory Comput.* **9**, 165 (2013).
- [8] T. Lelievre, M. Rousset, and G. Stoltz, *Free Energy Computations* (Imperial College Press, London, 2010).
- [9] D. J. Luitz, X. Plat, N. Laflorencie, and F. Alet, Improving entanglement and thermodynamic Rényi entropy measurements in quantum Monte Carlo, *Phys. Rev. B* **90**, 125105 (2014).

- [10] J. Preskill, Quantum Shannon theory, [arXiv:1604.07450](https://arxiv.org/abs/1604.07450).
- [11] T. M. Cover and J. A. Thomas, *Elements of Information Theory*, 2nd ed. (Wiley, Hoboken, NJ, 2005).
- [12] R. Horodecki and M. Horodecki, Information-theoretic aspects of inseparability of mixed states, *Phys. Rev. A* **54**, 1838 (1996).
- [13] G. Vidal, J. I. Latorre, E. Rico, and A. Kitaev, Entanglement in Quantum Critical Phenomena, *Phys. Rev. Lett.* **90**, 227902 (2003).
- [14] P. Calabrese and J. Cardy, Entanglement entropy and quantum field theory, *J. Stat. Mech. Theory Exp.* (2004) P06002.
- [15] M. M. Wolf, F. Verstraete, M. B. Hastings, and J. I. Cirac, Area Laws in Quantum Systems: Mutual Information and Correlations, *Phys. Rev. Lett.* **100**, 070502 (2008).
- [16] S. T. Flammia, A. Hamma, T. L. Hughes, and X. G. Wen, Topological Entanglement Rényi Entropy and Reduced Density Matrix Structure, *Phys. Rev. Lett.* **103**, 261601 (2009).
- [17] M. A. Metlitski, C. A. Fuertes, and S. Sachdev, Entanglement entropy in the $O(N)$ model, *Phys. Rev. B* **80**, 115122 (2009).
- [18] R. R. P. Singh, M. B. Hastings, A. B. Kallin, and R. G. Melko, Finite-Temperature Critical Behavior of Mutual Information, *Phys. Rev. Lett.* **106**, 135701 (2011).
- [19] E. Romera and Á. Nagy, Rényi entropy and quantum phase transition in the Dicke model, *Phys. Lett. A* **375**, 3066 (2011).
- [20] C. M. Herdman, S. Inglis, P. N. Roy, R. G. Melko, and A. Del Maestro, Path-integral Monte Carlo method for Rényi entanglement entropies, *Phys. Rev. E* **90**, 013308 (2014).
- [21] A. Kitaev and J. Preskill, Topological Entanglement Entropy, *Phys. Rev. Lett.* **96**, 110404 (2006).
- [22] R. Islam, R. Ma, P. M. Preiss, M. E. Tai, A. Lukin, M. Rispoli, and M. Greiner, Measuring entanglement entropy in a quantum many-body system, *Nature (London)* **528**, 77 (2015).
- [23] L. D'Alessio, Y. Kafri, A. Polkovnikov, and M. Rigol, From quantum chaos and eigenstate thermalization to statistical mechanics and thermodynamics, *Adv. Phys.* **65**, 239 (2016).
- [24] R. Nandkishore and D. A. Huse, Many-body localization and thermalization in quantum statistical mechanics, *Annu. Rev. Condens. Matter Phys.* **6**, 15 (2015).
- [25] F. Alet and N. Laflorencie, Many-body localization: An introduction and selected topics, *C. R. Phys.* **19**, 498 (2018).
- [26] T. Brydges, A. Elben, P. Jurcevic, B. Vermersch, C. Maier, B. P. Lanyon, P. Zoller, R. Blatt, and C. F. Roos, Probing Rényi entanglement entropy via randomized measurements, *Science* **364**, 260 (2019).
- [27] C. M. Herdman, P. N. Roy, R. G. Melko, and A. Del Maestro, Particle entanglement in continuum many-body systems via quantum Monte Carlo, *Phys. Rev. B* **89**, 140501(R) (2014).
- [28] J. Zhao, Y.-c. Wang, Z. Yan, M. Cheng, and Z. Y. Meng, Scaling of Entanglement Entropy at Deconfined Quantum Criticality, *Phys. Rev. Lett.* **128**, 010601 (2022).
- [29] H. Fan, V. Korepin, and V. Roychowdhury, Entanglement in a Valence-Bond Solid State, *Phys. Rev. Lett.* **93**, 227203 (2004).
- [30] G. Refael and J. E. Moore, Entanglement Entropy of Random Quantum Critical Points in One Dimension, *Phys. Rev. Lett.* **93**, 260602 (2004).
- [31] F. Franchini, A. R. Its, and V. E. Korepin, Rényi entropy of the XY spin chain, *J. Phys. A: Math. Theor.* **41**, 025302 (2008).
- [32] B. Bertini, P. Kos, and T. Prosen, Entanglement Spreading in a Minimal Model of Maximal Many-Body Quantum Chaos, *Phys. Rev. X* **9**, 021033 (2019).
- [33] N. Schuch, M. M. Wolf, F. Verstraete, and J. I. Cirac, Entropy Scaling and Simulability by Matrix Product States, *Phys. Rev. Lett.* **100**, 030504 (2008).
- [34] G. Vidal, Class of Quantum Many-Body States That Can Be Efficiently Simulated, *Phys. Rev. Lett.* **101**, 110501 (2008).
- [35] G. Carleo and M. Troyer, Solving the quantum many-body problem with artificial neural networks, *Science* **355**, 602 (2017).
- [36] M. Ceriotti, J. Cuny, M. Parrinello, and D. E. Manolopoulos, Nuclear quantum effects and hydrogen bond fluctuations in water, *Proc. Natl. Acad. Sci. USA* **110**, 15591 (2013).
- [37] A. P. Drozdov, P. P. Kong, V. S. Minkov, S. P. Besedin, M. A. Kuzovnikov, S. Mozaffari, L. Balicas, F. F. Balakirev, D. E. Graf, V. B. Prakapenka, E. Greenberg, D. A. Knyazev, M. Tkacz, and M. I. Eremets, Superconductivity at 250 K in lanthanum hydride under high pressures, *Nature (London)* **569**, 528 (2019).
- [38] P. Kong, V. S. Minkov, M. A. Kuzovnikov, A. P. Drozdov, S. P. Besedin, S. Mozaffari, L. Balicas, F. F. Balakirev, V. B. Prakapenka, S. Chariton, D. A. Knyazev, E. Greenberg, and M. I. Eremets, Superconductivity up to 243 K in the yttrium-hydrogen system under high pressure, *Nat. Commun.* **12**, 5075 (2021).
- [39] A. P. Drozdov, M. I. Eremets, I. A. Troyan, V. Ksenofontov, and S. I. Shylin, Conventional superconductivity at 203 kelvin at high pressures in the sulfur hydride system, *Nature (London)* **525**, 73 (2015).
- [40] F. Fillaux, Quantum entanglement and nonlocal proton transfer dynamics in dimers of formic acid and analogues, *Chem. Phys. Lett.* **408**, 302 (2005).
- [41] S. Miura, M. E. Tuckerman, and M. L. Klein, An *ab initio* path integral molecular dynamics study of double proton transfer in the formic acid dimer, *J. Chem. Phys.* **109**, 5290 (1998).
- [42] S. D. Ivanov, I. M. Grant, and D. Marx, Quantum free energy landscapes from *ab initio* path integral metadynamics: Double proton transfer in the formic acid dimer is concerted but not correlated, *J. Chem. Phys.* **143**, 124304 (2015).
- [43] M. Ceriotti, W. Fang, P. G. Kusalik, R. H. McKenzie, A. Michaelides, M. A. Morales, and T. E. Markland, Nuclear quantum effects in water and aqueous systems: Experiment, theory, and current challenges, *Chem. Rev. (Washington, DC)* **116**, 7529 (2016).
- [44] O. Pusuluk, G. Torun, and C. Deliduman, Quantum entanglement shared in hydrogen bonds and its usage as a resource in molecular recognition, *Mod. Phys. Lett. B* **32**, 1850308 (2018).
- [45] L. Amico, R. Fazio, A. Osterloh, and V. Vedral, Entanglement in many-body systems, *Rev. Mod. Phys.* **80**, 517 (2008).
- [46] C. Kinz-Thompson and E. Conwell, Proton transfer in adenine-thymine radical cation embedded in B-form DNA, *J. Phys. Chem. Lett.* **1**, 1403 (2010).
- [47] D. M. Ceperley, Path integrals in the theory of condensed helium, *Rev. Mod. Phys.* **67**, 279 (1995).
- [48] M. Tuckerman, *Statistical Mechanics: Theory and Molecular Simulation* (Oxford University Press, New York, 2010).
- [49] C. Chipot and A. Pohorille, *Free Energy Calculations* (Springer-Verlag, Berlin, 2007).
- [50] C. H. Bennett, Efficient estimation of free energy differences from Monte Carlo data, *J. Comput. Phys.* **22**, 245 (1976).

- [51] P. Broecker and S. Trebst, Rényi entropies of interacting fermions from determinantal quantum Monte Carlo simulations, *J. Stat. Mech.: Theory Exp.* (2014) P08015.
- [52] P. V. Buividovich and M. I. Polikarpov, Numerical study of entanglement entropy in $SU(2)$ lattice gauge theory, *Nucl. Phys. B* **802**, 458 (2008).
- [53] See Supplemental Material at <http://link.aps.org/supplemental/10.1103/PhysRevResearch.4.L032002> for additional information about the computational details for the quantum harmonic oscillator, the one-dimensional Ising model, and the *ab initio* calculations of the formic acid dimer. This includes Refs. [49,54,57–60].
- [54] G. B. Mbeng, A. Russomanno, and G. E. Santoro, The quantum Ising chain for beginners, [arXiv:2009.09208v1](https://arxiv.org/abs/2009.09208v1).
- [55] H. Tachikawa, Proton transfer vs complex formation channels in ionized formic acid dimer: A direct *ab initio* molecular dynamics study, *J. Phys. Chem. A* **124**, 3048 (2020).
- [56] M. M. Wilde, *From Classical to Quantum Shannon Theory* (Cambridge University Press, Cambridge, 2011).
- [57] F. Krzakala, A. Rosso, G. Semerjian, and F. Zamponi, Path-integral representation for quantum spin models: Application to the quantum cavity method and Monte Carlo simulations, *Phys. Rev. B* **78**, 134428 (2008).
- [58] H. W. J. Blöte and Y. Deng, Cluster Monte Carlo simulation of the transverse Ising model, *Phys. Rev. E* **66**, 066110 (2002).
- [59] Q. Sun, T. C. Berkelbach, N. S. Blunt, G. H. Booth, S. Guo, Z. Li, J. Liu, J. D. McClain, E. R. Sayfutyarova, S. Sharma, S. Wouters, and G. K. L. Chan, PYSCF: the Python-based simulations of chemistry framework, *Wiley Interdiscip. Rev.: Comput. Mol. Sci.* **8**, e1340 (2018).
- [60] Q. Sun, X. Zhang, S. Banerjee, P. Bao, M. Barbry, N. S. Blunt, N. A. Bogdanov, G. H. Booth, J. Chen, Z. H. Cui, J. J. Eriksen, Y. Gao, S. Guo, J. Hermann, M. R. Hermes, K. Koh, P. Koval, S. Lehtola, Z. Li, J. Liu *et al.*, Recent developments in the PYSCF program package, *J. Chem. Phys.* **153**, 024109 (2020).
- [61] <https://github.com/srdinsek/Renyi-Integration>.